PORTIONS OF THIS DOCUMENT ARE ILLEGIBLE

LA-UR -78-884

TITLE: STRUCTURE AND MECHANICAL PROPERTIES OF Al-Al_xO_y VACUUM DEPOSITED LAMINATES

AUTHOR(S): R. W. Springer and E. S. Catlett

SUBMITTED TO: International Conference on Metallurgical Coatings, San Francisco, CA, April 3-7, 1978

MN ONLY

los alamos
scientific laboratory
of the University of California
LOS ALAMOS, NEW MEXICO 87545

Form No. 836
St. No. 2629
1/75

UNITED STATES
ENERGY RESEARCH AND
DEVELOPMENT ADMINISTRATION
CONTRACT W-7405-ENG. 36

Structure and Mechanical Properties of Al-Al_xO_y Vacuum Deposited Laminates

by

R. W. Springer and D. S. Catlett
Los Alamos Scientific Laboratory
Los Alamos, NM 87545

ABSTRACT

High yield strength materials can be fabricated by many techniques. A method proposed by Koehler is to alternate thin layers of a high shear modulus material with that of a low shear modulus material. The layers must be less than one hundred atomic layers in thickness and be single crystals of similar lattice spacing epitaxially grown on top of each other. The mechanical effect would be to inhibit dislocation formation and mobility of dislocations through the solid. As such, the stress required to move a dislocation through the laminate can be on the order of one percent of the lower modulus material.

A novel technique has been developed to produce a laminate of Al-Al_xO_y by a Pulsed Gas Process (PGP) in an electron beam gun system. Samples of 25 micro-meters and thicker have been readily produced. The surface finish of the growing deposit appears to remain as smooth as the glass substrate. The tensile testing data show the material to obey a Hall-Petch relation for yield strengths of layer spacings of 50nM to 1200nM. The friction stress was measured directly from a pure vapor deposited sample at 27MPa. The K value was found to be .086 $MN/m^{3}/2$. These results could also be interpreted in terms of a sub-grain strengthening concept.

I. Introduction

The ability to provide increased strength to materials has been a subject of interest and study for many years. Modern metallurgical analysis has permitted many of the mechanisms to be identified and to allow a certain degree of quantification for calculation and prediction purposes. Among the various mechanisms for strengthening is that of precipitation hardening. The theory shows that the precipitates produce a drag and impeding effect on the dislocation movement, thus increasing the stress necessary to produce material yield. The relation governing this type of yield is the Hall-Petch[1] type shown in Eq. (1).

$$\sigma_Y = \sigma_o + Kd^{-n} \qquad (1)$$

The power of n is ~-1/2 for this type of strengthening. The average precipitate spacing is the value of d in the equation.

In addition to the precipitation hardening there are two other forms, closely related to each other, which are grain boundry and sub-grain hardening. Both of these mechanisms are predicted on the fact that dislocation movement is impeded at an interface such as a grain boundary or a small tilt boundary within a grain itself. The grain boundary or sub-grain structure may impede or stop the movement of a dislocation but the material may still be subject to a low yield stress. It has been suggested that the dislocation which stopped at a hardened site or grain boundary, can cause a new dislocation to be generated at the other side, or activate an existing dislocation to move without actually penetrating the barrier.[1]

Examples of the first type of strengthening mechanisms in vapor deposited materials can be found in the work by McClanahan et al.[2] for precipitation hardening. Alloy targets were sputtered onto the substrates that were subsequently heat treated to cause precipitation. Grain boundary hardening was carried out by Merz and Dahlgren[3] in pure copper deposits. They obtained a very good fit to a Hall-Petch relation with the power n equal to -1/2 in accordance with current grain boundary theories.

A theory proposed by Koehler[4] suggests a slightly different approach to the material strengthening problem. The material is to be composed of a lamellar structure of material A and material B. The elastic constants of the two materials must differ by more than a factor of two. The two materials should also have the same crystal structure and lattice constants. Under these conditions, material A is deposited as a single crystal to a layer thickness of ~100 atom layers or less, followed by an epitaxial layer of the second material to the same thickness and so on until a composite material of macroscopic dimensions is produced. The single crystal requirement is necessary to avoid the presence of any dislocations, and the lattice constant requirement is to minimize the effect of interfacial strain. With this structure, a dislocation must form in a loop, since there is no grain boundary or imperfection for the dislocation to begin and end. The layer thickness is such that the minimum size loop is not easily formed. Thus, only partial loops may be formed. With these assumptions, Koehler calculates the line energy and shear required to force a dislocation through the couple from the lower modulus material to the higher modulus material. The result is shown in Eq. (2).

$$\mu_{min} \sim \frac{\mu_B}{8\pi}\left(\frac{\mu_A-\mu_B}{\mu_A+\mu_B}\right) \qquad \mu_A > \mu_B \tag{2}$$

Lehoczky[5] shows that for a dislocation moving on a glide plane in metal B to metal A, the minimum stress required for yield is given by Eq. (3) for equal thickness layers.

$$\sigma_Y' \sim \frac{1}{2}\left(1+\frac{Y_A}{Y_B}\right)\frac{\mu_B}{8\pi}\left(\frac{\mu_A-\mu_B}{\mu_A+\mu_B}\right) \tag{3}$$

Y_A and Y_B are the Young's moduli of the respective materials, while the A and B are the shear moduli of the materials. By inserting various material constants into Eq. (3), it can be seen that a composite of very high yield strength could be produced.

Numerous workers have made laminates in this fashion. Palatnik[6] made laminates of Ge and GaAs, Busch and Patten[7] looked at a variety of laminates including Be/Al, Lehoczky[5] investigated Al/Mg, Al/Cu and Al/Ag laminates including a few other systems. The laminates produced by Busch et al. were all subject to premature fracture and therefore yield strengths were inferred from hardness data. Lehoczky was able to measure specimens and obtain yield and ultimate tensile strength data. However, his data is somewhat difficult to interpret as he measured the mechanical properties as a function of constant stress rate rather than constant strain rate. Under these conditions, perameters such as ductility could not be investigated. In any case, the yield strengths were on the order of the values computed from Eq. (3) for laminate thickness of less than 50nM per layer.

Another laminate combination that would produce a high strength material is Al/Al_2O_3. At least two problems in forming such a laminate by electron beam gun evaporation would be encountered. First, a two gun system is required. Secondly, the possibility of electron stimulated desorption of the oxygen from the Al_2O_3 compound would produce a deficient oxide with an unpredictable stoichiometry.[8] However, recent work[9] investigated the effect of gas interaction with aluminum deposits condensed on room temperature substrates. In this study six gases were admitted to the chamber. Of the H_2O, O_2, N_2, CO, CO_2 and CH_4, only H_2O and O_2 were found to have any significant interaction with the deposit. The amount of oxygen found in the films followed the relation of Eq. (4) over two orders of magnitude of pressure variation.

$$O/Al = k \sum_i \lambda_i(\theta, T) \frac{R_{gi}}{R_d} \qquad (4)$$

The value k is a geometric factor to compensate for the difference in the measured pressure and the true pressure at the substrate. λ_i is the sticking probability for the gas atoms as a function of coverage, θ, and temperature (T). R_{gi} is the flux of gas atoms to the substrate and R_d is the flux of aluminum deposit to the substrate. It is thus apparent that using gas to form the Al_xO_y layer, it is possible to precisely control the oxygen content in the oxide layer. It is also possible then to produce layers highly deficient in oxygen to fine tune the desired mechanical properties of the laminate such as strength and ductility.

A. Experimental

Laminate composites of Al/Al_xO_y have been prepared in an electron beam gun deposition system. The system is all stainless steel and pumped by a Balzers 400 1/s turbo-molecular pump. An ultimate pressure of 1.4×10^{-6} Pa is attainable with this system. The electron beam gun system is a 14 KW Airco Temescal unit with a water cooled copper super hearth gun. The 5n's pure aluminum was deposited from the hearth without the use of a liner at a rate of ~3.5 nm/s.

For long runs and high gas pressures, certain modifications in the electron beam gun control circuitry were found to be advantageous. Figure 1 shows schematically the changes implemented. During the electron beam evaporation, positive ions are produced near the hearth by the incident high energy electrons. These ions are then collected on a negatively biased plate mounted on the electron beam gun. This current is measured and compared with a control setting. The subsequent error signal is amplified and fed to the emission control power circuit. Thus, the rate of deposit is maintained at a constant value throughout the run. However, problems can arise as the gas is pulsed into the system to form the oxide layer in that the gas may also be ionized by the electron beam and these ions collected and measured by the sensor plate. This artifact signal then causes the electron beam gun to shut down. However, this difficulty is easily overcome. A fraction of the signal from the ionization gauge, when in the 10^{-2}Pa region, is also fed to the current sensor. Thus, the effect of increased current due to the ionization of the gas is compensated by the ionization gauge reading.

The gas is pulsed into the chamber using the scheme shown in Figure 2. A high purity oxygen gas bottle is connected to a regulator, with a variable leak valve connected between two solenoid valves. The solenoid valves are connected to a relay driven by an oscillator circuit. The oscillator can be adjusted for cycle length as well as the relative duty cycle for gas admission. In this fashion, both the oxygen layer thickness, oxygen concentration and layer spacing are independently adjustable.

The working curve for the gas operation is shown in Figure 3. The data points shown are the oxygen to aluminum atomic ratios as measured by Auger Electron Spectroscopy. The abscissa is the mass 32 current as measured by a quadrapole residual gas analyzer. The line

is a plot of Eq. (4) using literature values of the sticking coefficient of oxygen on aluminum. The only information that cannot be obtained from this data is the instrument response to a spike of gas pressure admitted to the operating chamber. The gas diffusion plus reaction will cause the leading edge of the spike to be slightly sloped in time, and the ability of the vacuum system to recover, including the self-cleaning of the source, will cause a decay slope. This response time of the system limits the effective resolution of deposit and layer spacing as will be seen in the data.

The mechanical specimens were made by depositing through a "dog bone" shaped mask onto a glass lantern slide. Prior to the deposition of the laminate, a thin layer of CsI~50nm thick was deposited as a parting agent. During the deposition of the laminate, the mass 32 ion peak was plotted on a strip chart to record the number of cycles, the frequency and the intensity of the oxygen signal. The thickness of the specimens was measured both by a quartz crystal monitor, which could also display the deposition rate, and by the film step height using the syslus technique.

The samples were then "released" from the substrate by immersing the slide into water. The mechanical specimens were then "floated" off the glass, thoroughly rinsed and dried.

B. Chemical Analysis

The specimens were analyzed for oxygen content utilizing Auger Electron Spectroscopy and depth profiling techniques. The depth profiles were obtained using Tailored Modulation Techniques (TMT)[10] to eliminate the usual artifact for aluminum concentration found in dN/dE spectra at oxide interfaces.[11] A depth profile of both a 90nm spacing and 189nm spacing are shown in Figure 4. The oxygen concentration in the two profiles is roughly 5-10 atomic percent. So, the layers are highly oxygen deficient. However, the necessary reasons for this will be explained later in the machanical testing section.

Note in the profiles that the shapes of the oxygen layer are regular but very much broader than the oxide layer on the outer surface. Of particular importance is the shape and width of the peak in Figure 4a. The oxygen shape in this layer is determined solely by the instrument response to the gas as this film was formed. The oxygen was "pulsed" into the chamber. It is clear from this profile that the minimum spacing of layers can only be ~50nM before significant interference of the oxygen layers occur with the loss of metallic behavior in between.

It can be seen from the depth profile data that the material can be layered using the Pulsed Gas Process (PGP). Also, it should be observed that the concentration of oxygen and oxygen shape distribution can be controlled and are extremely uniform. Another way of observing the uniformity of the layering is shown in Figure 5. Scanning Auger images of "metallic" aluminum and oxygen concentrations are shown in the sputtered area. Each ring represents a change in film height of ~25nM. This effect is due to the Gaussian shape of the sputter beam used for depth profiling.

Most of the specimens measured for stress-strain values were depth profiled. The layer spacings found from the Auger analysis were found to be consistent with those recorded during the time of deposition.

C. Metallography

A 25 micrometer thick sample was mounted and polished. The layer spacing of this sample was ~200nM. The oxygen concentration was ~5-10 atomic percent. The polished section revealed no structure under the optical microscope. This is in sharp contrast to the pure aluminum deposits also examined. The structure revealed in these deposits is characteristic of a columnar structure consistent with the model of Movchan and Demchischin.[12] Upon etching, the structure revealed is shown in Figure 6. The one plate shows scanning electron microscopy at normal incidence. The appearance of this plate is similar to gray phases in a precipitate hardened sample. However, upon examination at 45°, it becomes apparent that the gray phases are in fact layers of oxide that were not etched away. It is clear that the periodic chemical changes in the sample have radically altered the structure of the material into a lamellar construction.

X-ray diffraction on this sample also showed that there was no preferred orientation. This is also in contrast to pure deposits which show a preferred 111 orientation. The crystallite size in this material must be in excess of 150 nM as no discernable broadening of the X-ray lines over instrumental was observed.

In addition to the difference in crystal orientation and structural changes, the surface morphology of the laminate is significantly different. Figure 7 shows the surface of a 12 micron thick laminate. The surface roughness of the pure aluminum has been recognized

by other workers.[13] The most striking feature of the laminate is its visual appearance. As the SEM plate shows, the surface is very smooth. The foil appears as reflective on the growing side as the glass or substrate side. This effect is reproduceable and appears to correlate with laminate spacings of 200nM or less. For the larger spacing, the growing side of the deposit begins to "roughen" as with the pure deposits.

D. Mechanical Properties

The stress-strain curves were obtained from two machines. One was a commercial Instron. The other was specially constructed to test the thin foil specimens. Figure 8 shows the schematic operation of the second machine. Both machines were of the constant strain rate type and data compared between the two was in good agreement. The strain rate used was $\sim 5 \times 10^{-5}$/s. The specimens averaged ~7-10 microns thick, ~3mm wide and had a gauge length ~2cm. The samples were glued to stainless steel strips ~1 cm wide by ~.13mm thick used as pull grips.

Table I shows the results of the mechanical testing. All the yield strengths were measured at the .2% offset point. In the table is shown the yield strength, ultimate tensile strength, elongation, layer spacing and relative oxygen concentration. If a Hall-Petch relation is obeyed, the data should fall on a straight line on a log-log plot of the yield strength versus the laminate spacing. Figure 9 shows such a plot. The data fit an experimental line of slope-1/2. A replot of the yield stress data versus a reduced axis of $d^{-1/2}$ gives Figure 10. Included in this plot is the yield strength for the pure aluminum deposit. As can be seen from the plot, the σ_0 term from the best experimental fit agrees very well with the yield stress measured for pure aluminum samples.

E. Results and Discussion

The yield stress predicted by Eq. (3) is about 5.5 times larger than the maximum yield stress experimentally measured. This discrepancy is not at all surprising in light of the fact that the computation is based on elastic perameters of pure alumina. The mechanical specimens had reduced oxygen content to eliminate brittle fracture due to internal stresses and to introduce ductility. Assuming that the 5-10 atomic percent oxygen increased the elastic constant of that layer over pure aluminum by about two times, one computes 446 MPa or about the yield strength of the 50 nM spaced specimen.

The material could be described in terms of a sub-grain hardening mechanism as well. The Hall-Petch coefficients match those of sub-grain hardened aluminum better than grain boundary hardening.[1] This assumption would agree well with the x-ray diffraction data showing no line broadening on lamallae spacing of 200 nm. In the sub-grain hardening theory, the value of K in Eq. (1) can be computed. However, the details and mechanisms involved in such a computation is still the subject of controversy. The general form of most of the results is shown in Eq. (5).[1]

$$K = \frac{G\bar{b}}{2\pi(1-\nu)}\left[\frac{8\theta}{\pi\bar{b}}\right]^{1/2} \qquad (5)$$

Where G is the shear modulus, $\bar{b}$ is the Burgers vector, ν is Poisson's ratio and θ is the angular pile up of dislocations in the sub-grains. For an angular mismatch of ~20° and a Burgers vector of one lattice spacing, Eq. (5) yields a value of $\sim .09 MN/m^3/2$ which is extremely close to the value measure in this experiment and others involving sub-grain hardening.[1]

The mechanical properties compare favorably with electrodeposited aluminum[14] dispersion hardened with alumina particles. The sintered and pressed alloys made from the fine particles of aluminum are also high in oxygen content. The laminate strengths are comparative to this class of XAP alloys.[15]

Conclusions

The PGP offers a chance to control many material perameters in a precise and repetitive manner. The strength enhancement of aluminum has been shown to be achieved by the alternation of oxidized layers and metallic layers. The bond strength of the layers, although not measured, is thought to be very high as delamination was found to be very rare and not observed in samples subjected to liquid nitrogen temperatures or elevated temperatures ~300C. This is thought to be due to the bond strength of the grown oxide.

The mechanical behavior of the material is described by the Hall-Petch relation with a friction stress of 27MPa and a K value of $\sim .085 MN/m^3/2$. The ductility of the material appears to be inversely related to the yield strength with the elongation ranging from ~20% to less than .2% for the strongest sample.

Some microleveling must be achieved during the layering process as the usual surface roughness found on thick aluminum deposits was suppressed.

In conclusion, the PGP can produce aluminum coatings showing desirable properties of controlled enhanced mechanical strength with reduced to non-existent surface roughening effects.

Acknowledgements

The authors would like to thank Dr. G. Hurley for the many valuable discussions concerning the mechanical testing. B. Barthell is thanked for his help in assembling the mini-tensometer. Finally the authors wish to thank C. Javorsky for the metallography and SEM work.

References

1. R. J. McElroy and Z. C. Szkopiak, Int. Met. Rov., 17, p. 175, (1972).
2. E. D. McClanahan, R. Bush and R. W. Moss, NASA Tech. Report CR-134542,(1973).
3. M.D. Merz and S. D. Dahlgren, J.AP, 46, no.8, 3235, (Aug.1975).
4. J. S. Koehler, Phys. Rev. B, 2, 547, (1970).
5. S. L. Lehoczky, Navy Tech. Report MDC Q0593, (1976).
6. Palatnik, Utr. Fiz. Zh., 16, no.12, 2077-9, (Dec. 1971).
7. R. A. Busch and J. W. Patten, ARPA Tech. Rep. No. 2482-2, (1975).
8. M. Knotek and P. J. Feibelman, in press for Phys. Rev. Lelt.
9. R. W. Springer and D. S. Catlett, JVST, 15, No.2, (1978).
10. R. W. Springer and D. J. Pocker, Rev. Sci. Inst., 48, no. 1, P74(1977).
11. J. T. Grant, T. P. Hooker, R. W. Springer and J. W. Haas, JVST 14, no.1, p. 32 (1977).
12. B. A. Movchan and A. V. Demchischin, Fiz. Metall. Metalloved., 28, <53 (1969).
13. N. G. Dhere etal., Thin Solid Films 30, 267 (1975).
14. K. R. Van Horn, Editor, Aluminum (Chapman and Hall, London, 1967), Vol. 2.

TABLE I

D (nM)	Ys MPa	UTs MPa	ϵ %	~O atomic %/layer
50	408	408	.2	3
90	326	434	.5	8
110	262	300	5	7
132	265	293	2	10
144	252	265	4	5
144	234	272	7	5
189	245	286	2	7
206	252	312	10	___
245	250	312	.5	7-15
292	182	236	15	3
319	172	225	7	___
330	173	212	7	4
349	156	204	3	___
1200	109	131	20	___
00	22	78	30	0

Figure Captions

1. The schematic of the rate control circuit is outlined. The ions created by the electrons are collected and compared to a reference signal. The difference is amplified and used to control the deposition. A part of the ionization gauge signal is also fed into the controller to compensate for gas ions created at the 10^{-2}Pa pressure region.

2. The gas inlet system is shown in block diagram. The oscillator is both cycle as well as pulse width adjustable to control the layer spacing and oxygen layer thickness.

3. The working curve for oxygen reactions with aluminum is shown. The solid line is a calculation from Eq. (4) with K 2.3, $\theta \sim .03$ and a depositon rate of 1.5nM/s. The pressure is $\sim 10^{-2}$Pa at 10^{-8} amps of RGA current. The circles are the oxygen to aluminum atomic ratios as measured by Auger Electron Spectroscopy.

4. Two oxygen depth profiles are shown. The beginning of the curves represent the relative thickness of the oxide layer at the surface of the samples. Note the uniformity of the oxygen spacing in both profiles. The total sputter time shown is about 80 minutes with ~1μ material removed. Trace A is for a laminate spacing ~90nM. Curve B is for a laminate spacing ~189nM. Note that the resolution of the oxygen layer in this plot degrades with time due to the imperfect alignment of the sputter beam with the electron beam.

5. A. An SEM type image of the Gaussian sputter crater reveals a uniform ringed pattern. Each band corresponds to a change in depth of ~25nM. B. An Oxygen Scanning Auger Micrograph (SAM) shows the light bands in A to be the oxide layers. C. An aluminum SAM on the "metallic" aluminum peak is complimentary to plate B and corresponds to the dark bands in A.

6. Scanning Electron Microscopy of the edge of a polished and etched sample is shown at two different angles. It is very clear that layering has been achieved and the usual columnar structure is gone.

7. The effect of layering by the PGP on the surface roughness is seen in this pair of SEM micrographs. A is the surface of the laminate and B is the rough surface of a pure deposit. Both samples are 12u thick.

8. A schematic block diagram of the special tensometer is illustrated. A ramp is generated, compared to the signal from a differential transformer used as a strain gauge. The resultant signal is fed to a power amplifier to drive the solenoid. The total force that can be developed by this machine is 9.8N.

9. A log-log plot of the yield stress versus the layer spacing gives essentially a straight line. The line has a slope ~-1/2.

10. The yield stress and layer spacing are plotted on a linear ordinate and reduced abscissa. It is interesting to note that the experimental line intersects the yield stress for a pure specimen. The equation gives the yield stress in MPa for 5-10 atomic percent oxygen in the oxide layer.

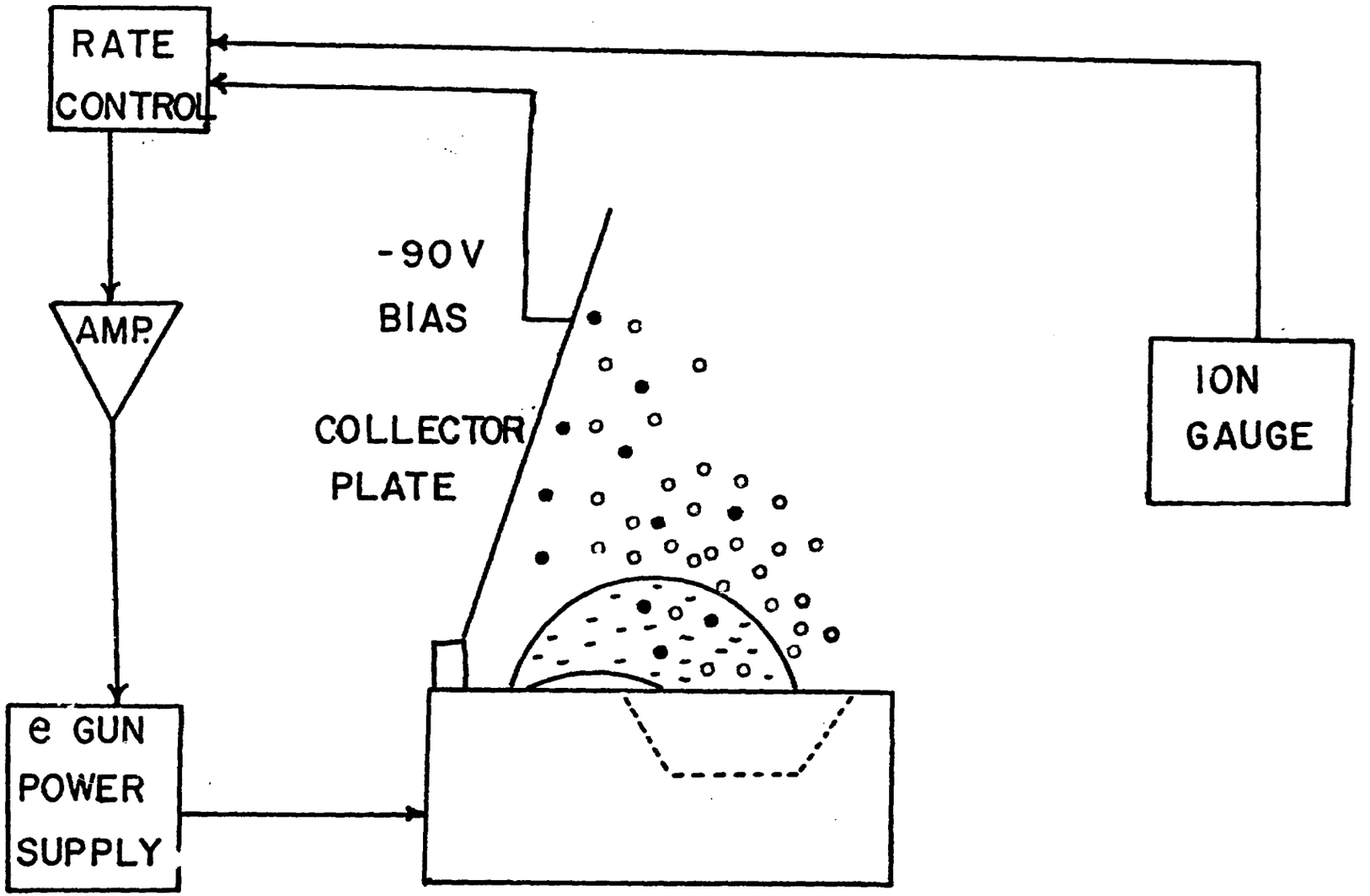
RATE
CONTROL
AMP.
-90V
BIAS
COLLECTOR
PLATE
ION
GAUGE
e GUN
POWER
SUPPLY

e⁻ GUN

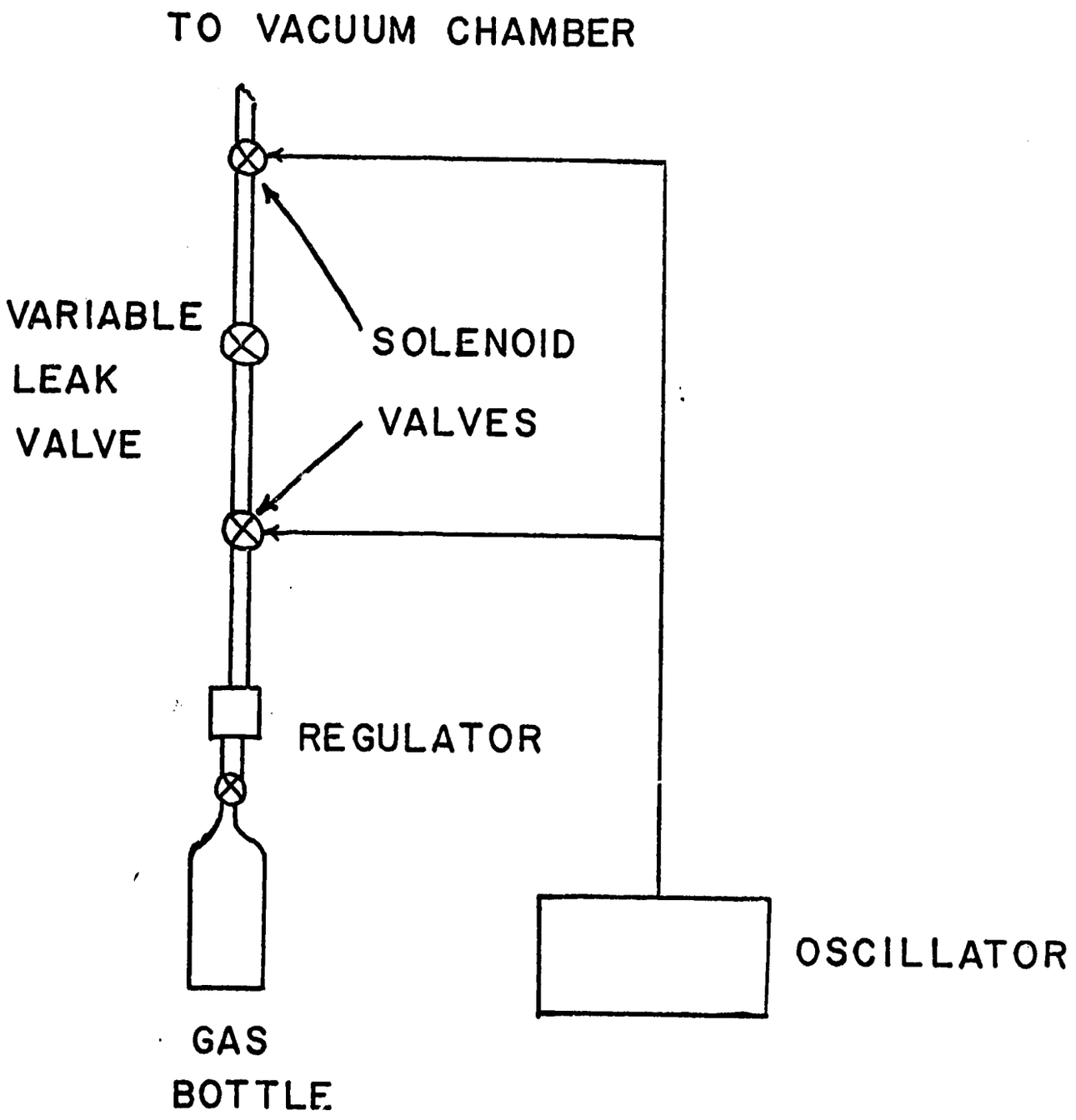
TO VACUUM CHAMBER
VARIABLE
LEAK
VALVE
SOLENOID
VALVES
REGULATOR
OSCILLATOR
GAS
BOTTLE

Fig 2

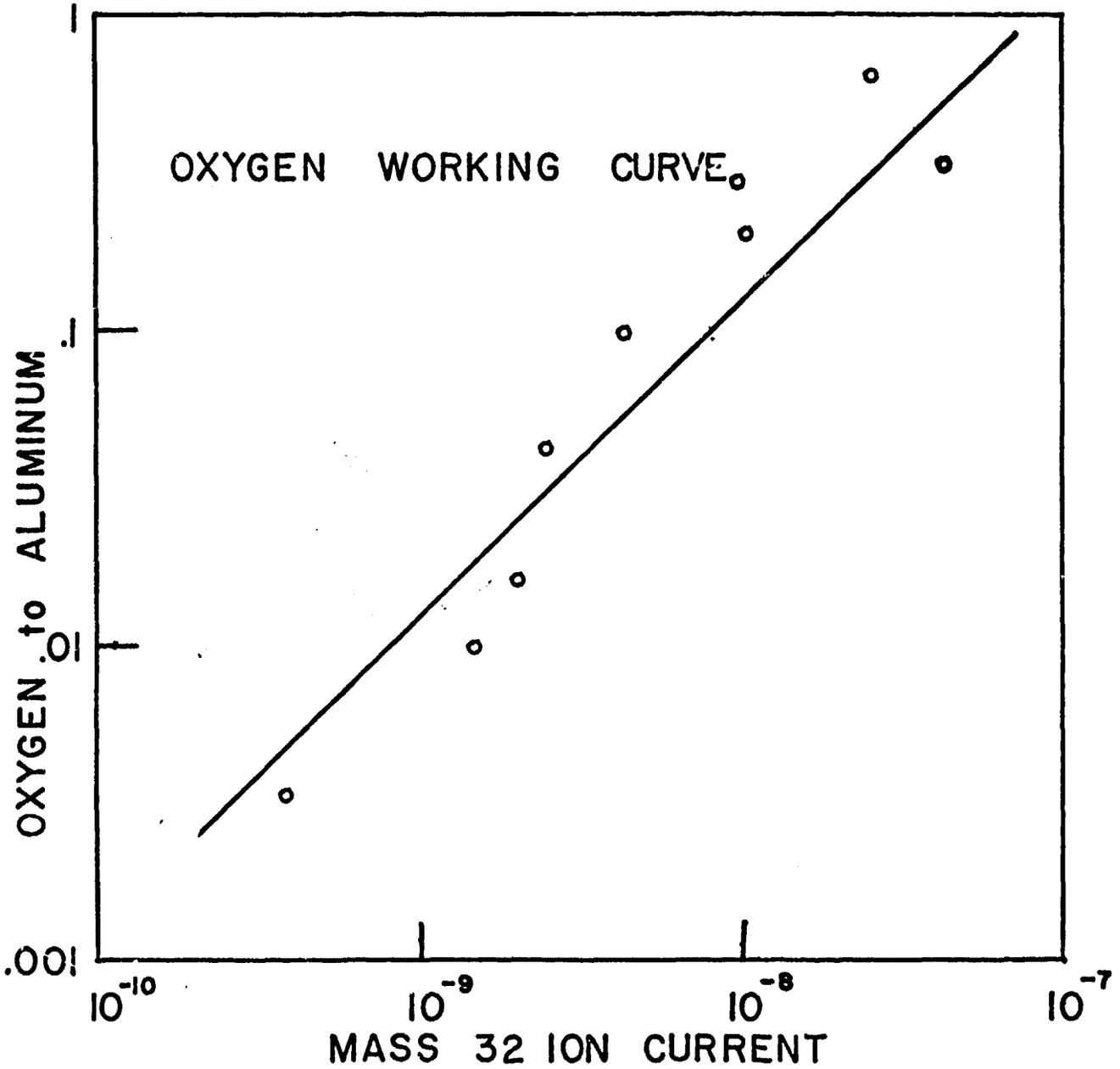
OXYGEN WORKING CURVE
OXYGEN to ALUMINUM
1
.1
.01
.001
10^{-10}
10^{-9}
10^{-8}
10^{-7}
MASS 32 ION CURRENT

Fig 3

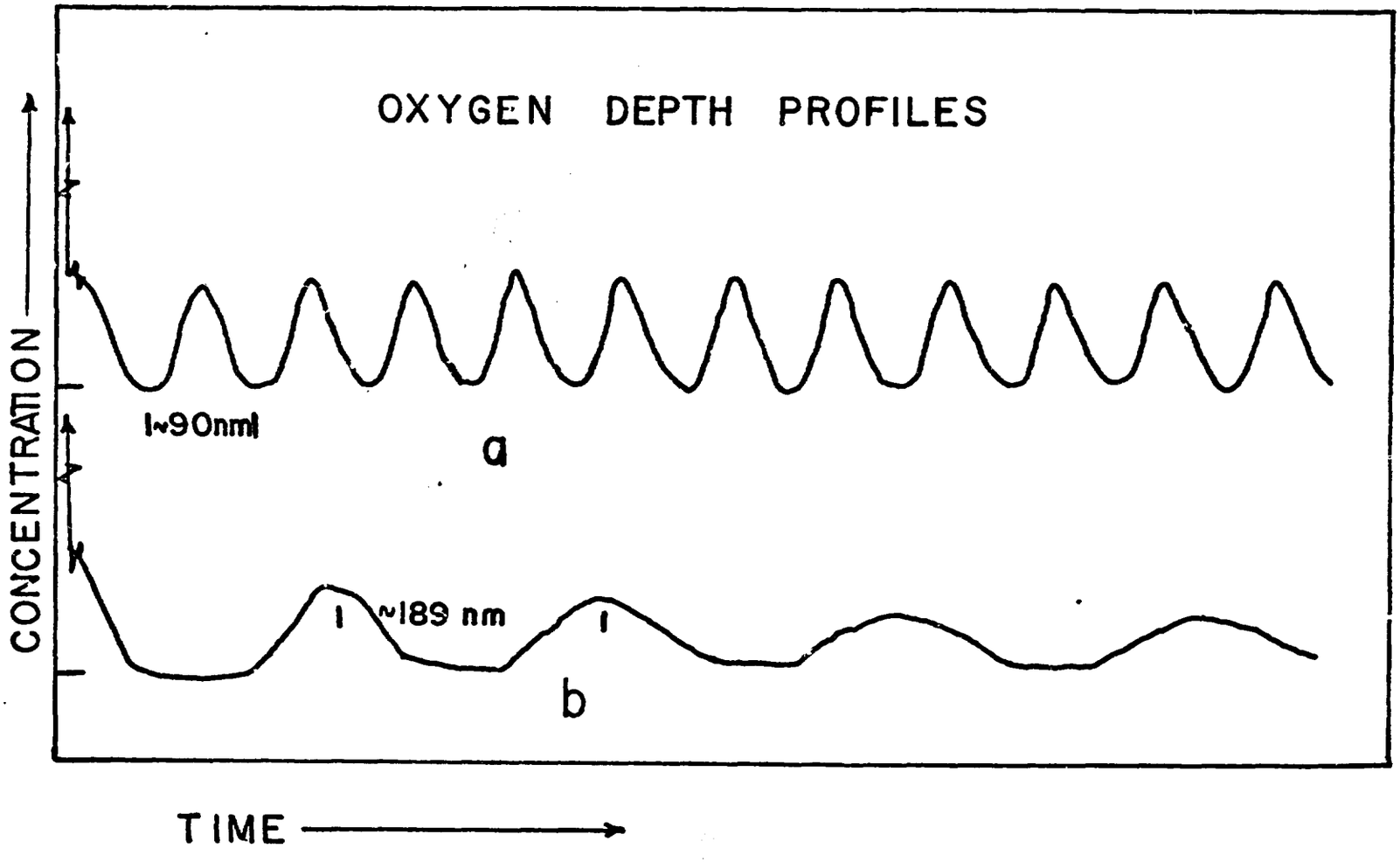

Fig 4

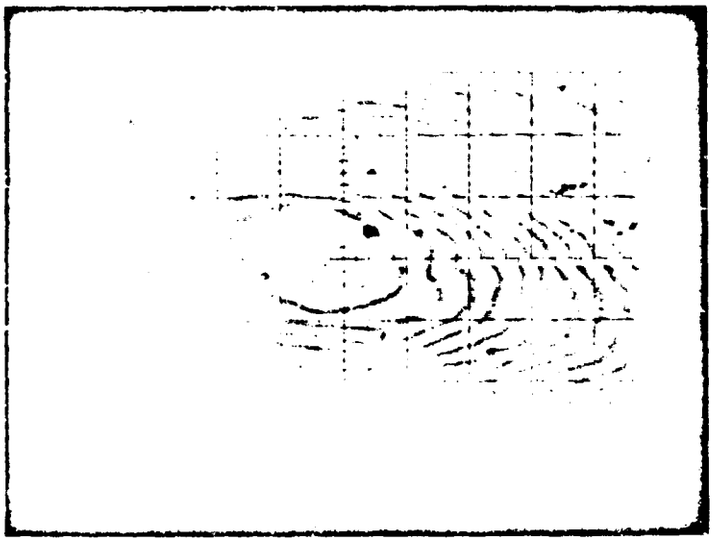

A Adsorbed Current ~60x

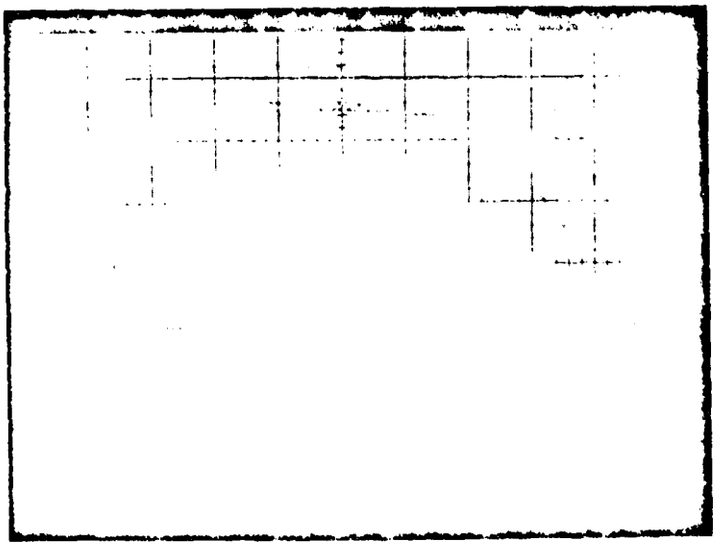

B O SAM 250x

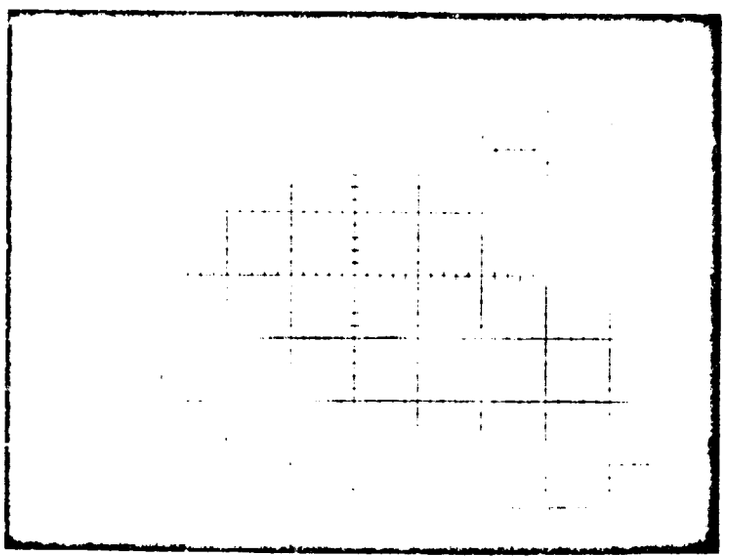

C Al SAM 250x

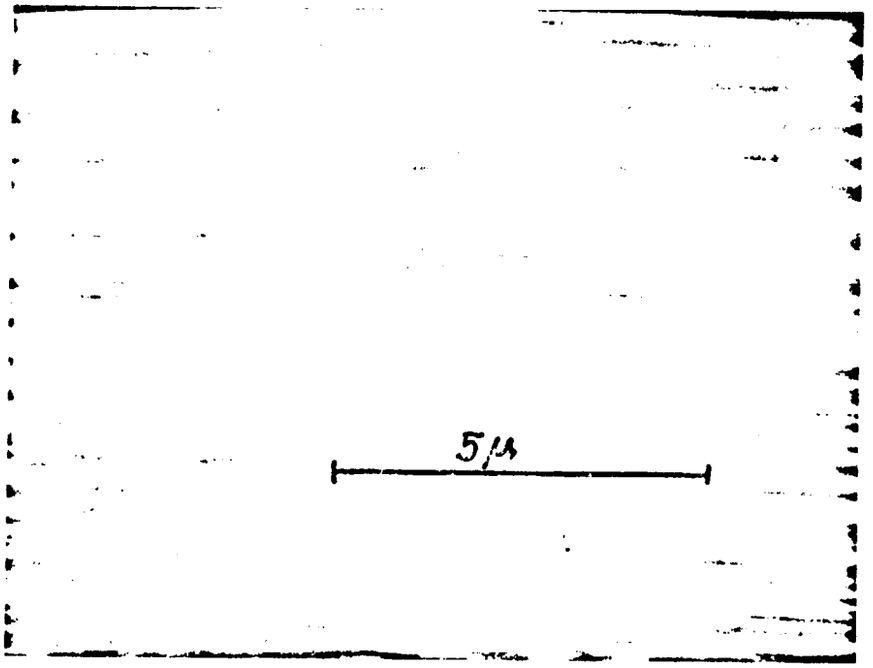

A SEM AT 0°

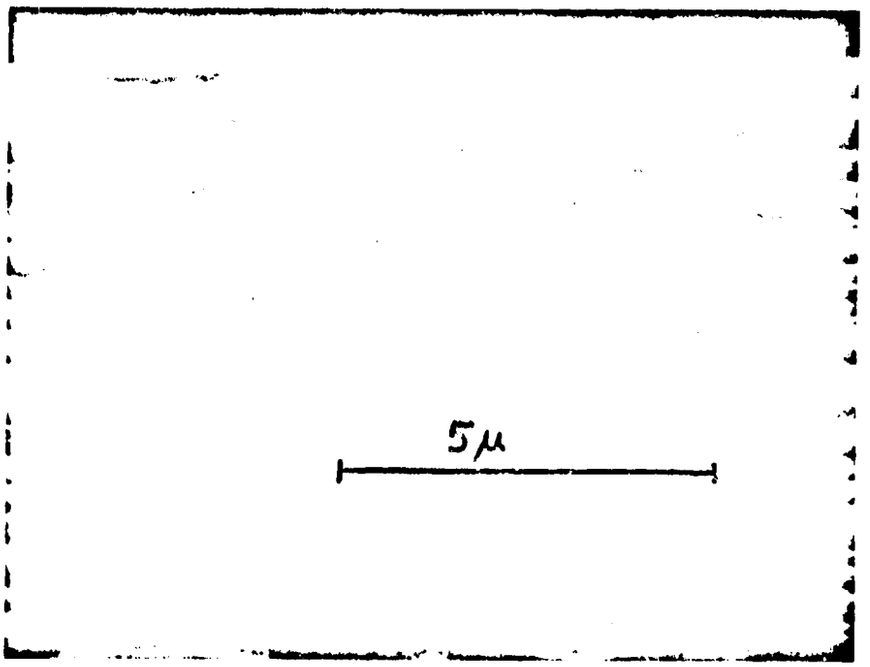

B SEM AT 45°

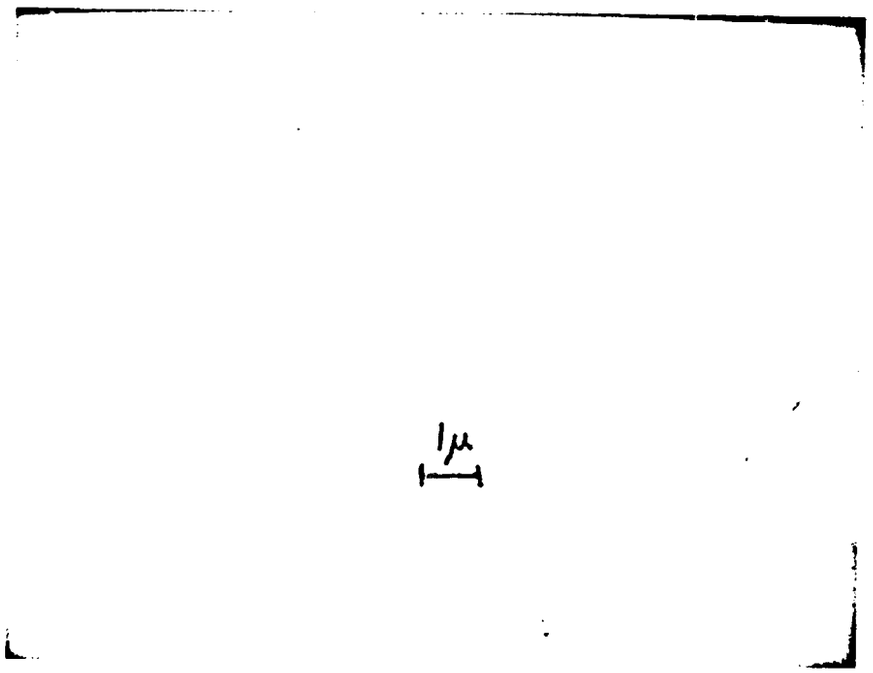

A SURFACE OF LAMINATE

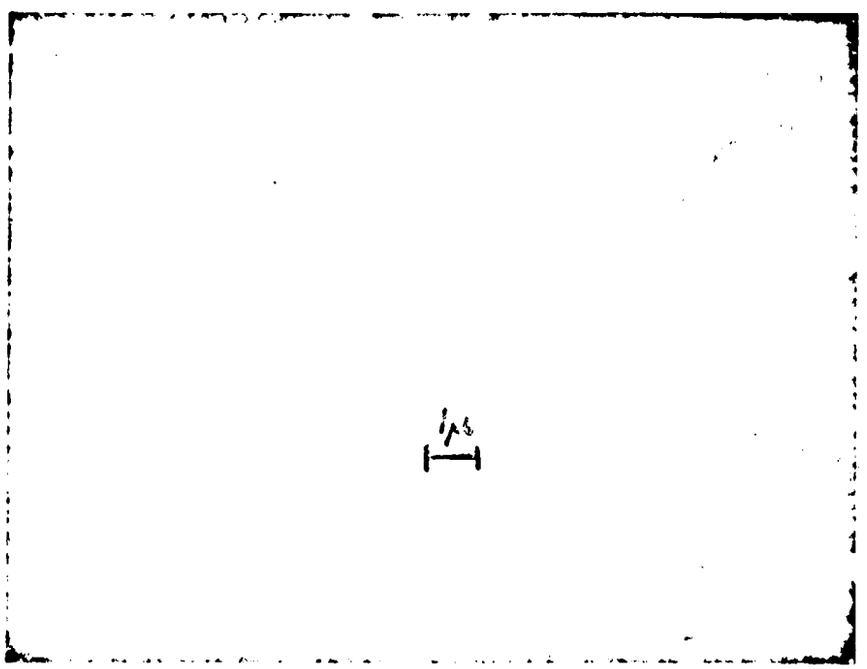

B SURFACE OF PURE Al DEPOSIT

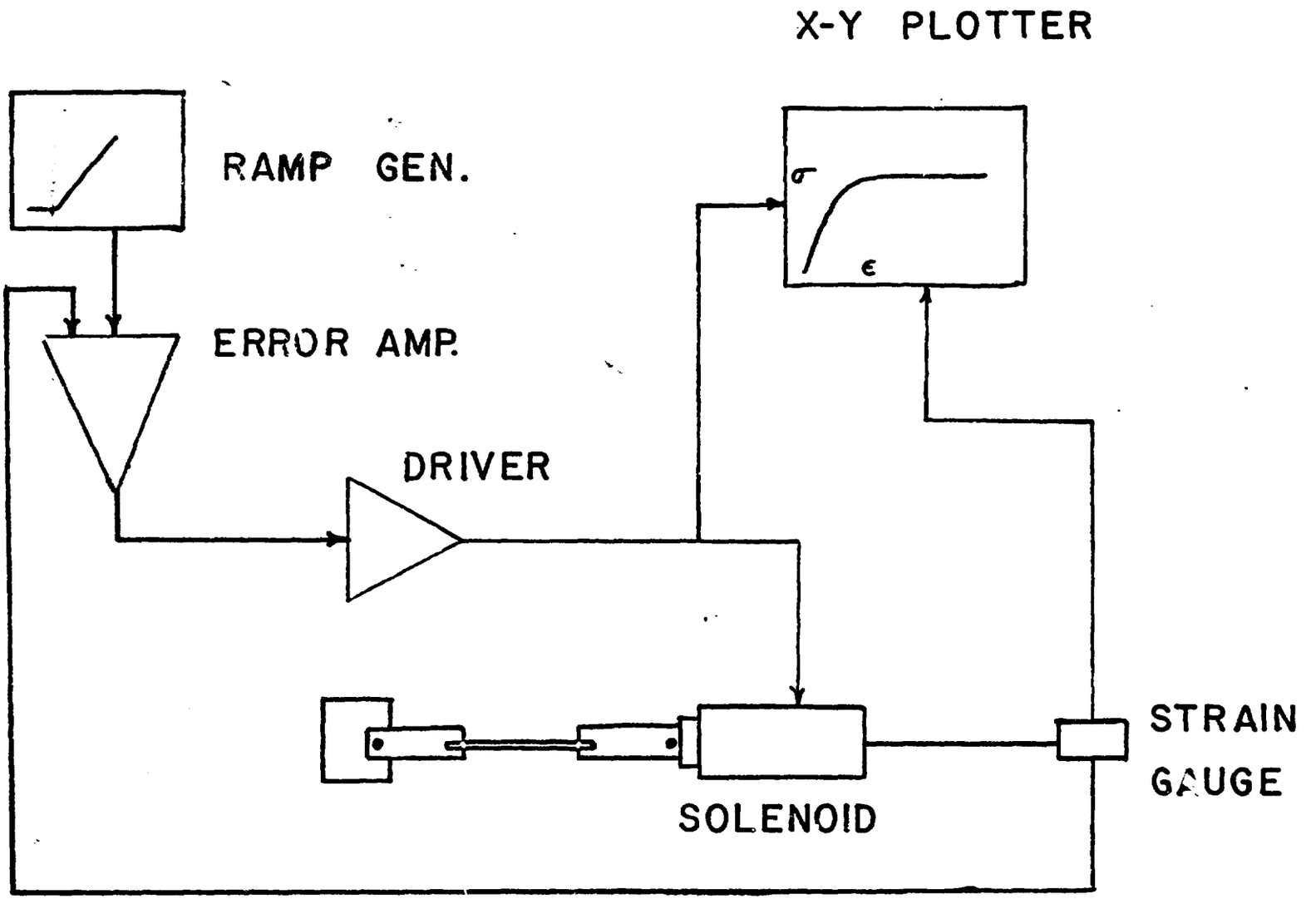
X-Y PLOTTER
RAMP GEN.
σ
ε
ERROR AMP.
DRIVER
STRAIN
GAUGE
SOLENOID

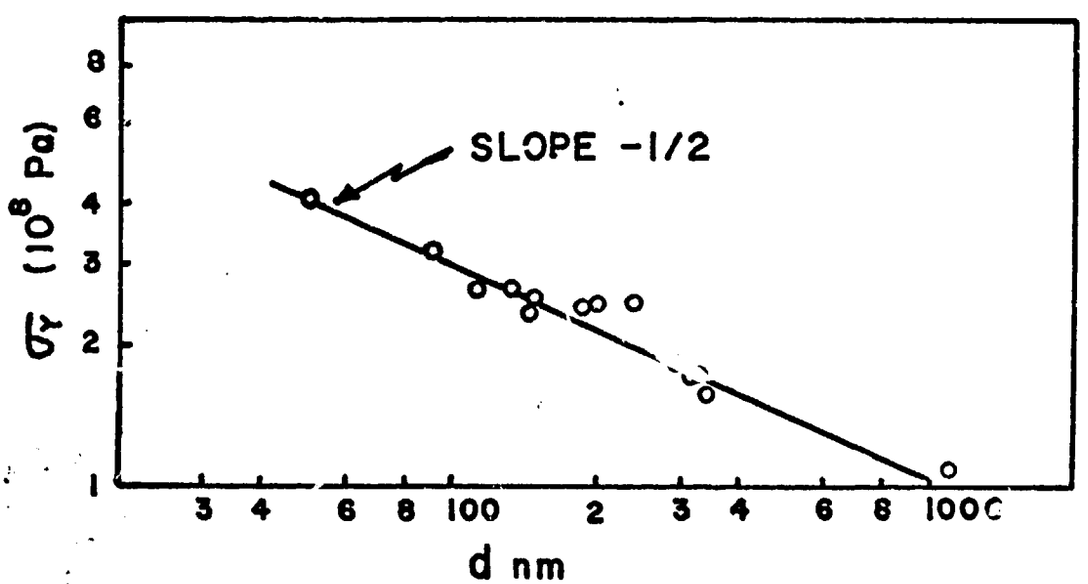

Fig 1

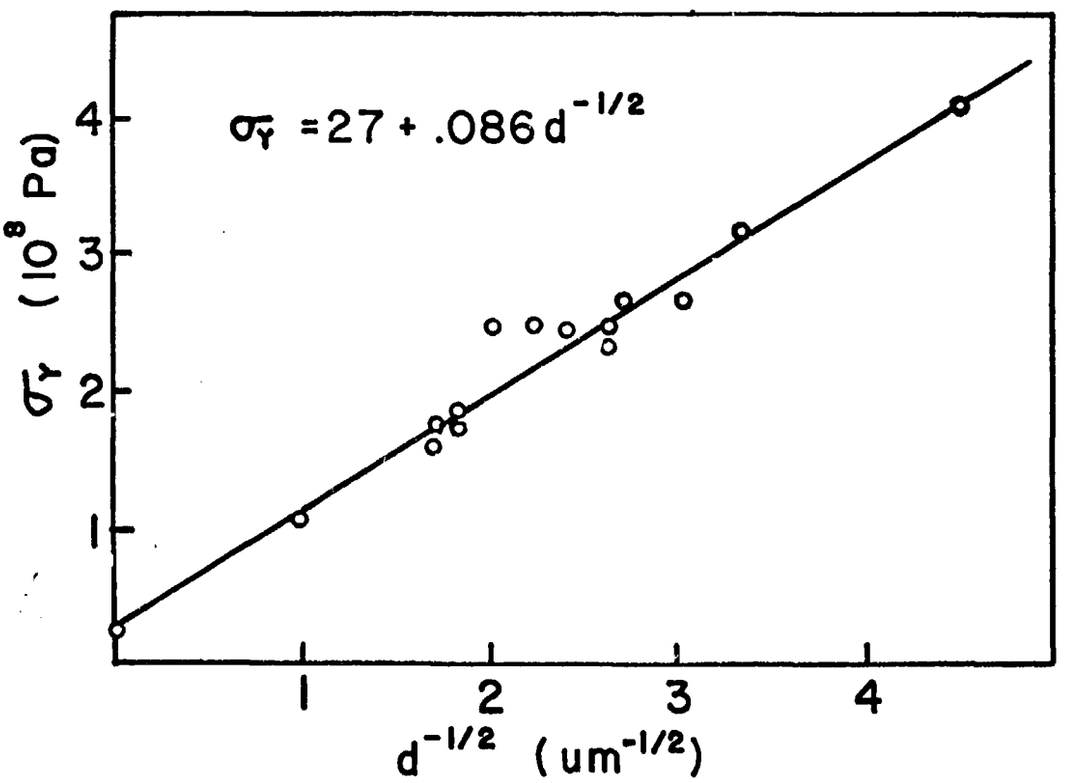

F. 8 10